

# Microscope for X-ray orbital angular momentum imaging

Yoshiki Kohmura,<sup>1</sup> Kei Sawada,<sup>1</sup> Masaichiro Mizumaki,<sup>2</sup> Kenji Ohwada,<sup>3</sup> and Tetsuya Ishikawa<sup>1</sup>

<sup>1</sup>RIKEN, SPring-8 Center, 1-1-1, Kouto, Sayo-gun, Sayo-cho, Hyogo 679-5148, Japan

<sup>2</sup>Japan Synchrotron Radiation Research Institute, 1-1-1 Kouto, Sayo, Hyogo, 679-5198, Japan

<sup>3</sup>National Institutes for Quantum and Radiological Science and Technology (QST),  
1-1-1, Kouto, Sayo-gun, Sayo-cho, Hyogo 679-5148, Japan

Orbital angular momentum (OAM) of photons is carried upon the wave front of an optical vortex and is important in physics research due to its fundamental degree of freedom. As for the interaction with materials, the optical OAM was shown to be transferred to the valence electron based on modified selection rules where a single ion is carefully aligned to the center of a vortex[1]. We here demonstrate an elaborate way of extracting the distributed OAMs in the two-dimensional x-ray wave field at the exit-face of the specimen by a vorticity-sensitive microscopy, which detects vorticity in the reciprocal-space wave field downstream of the optical vortices. This method enables us to measure the distributed topological charges and OAMs by a single image with the wide field of view over 300  $\mu\text{m}$ . Among various wavelength, the research of x-ray OAM is especially interesting since it could be closely related to the predicted OAM-induced x-ray dichroism[2].

The intensity profile with a central zero, around an optical vortex, is elaborately utilized in a modern super-resolution microscope[3, 4] and in nano-fabrication well under the scale of the diffraction limit[5–9]. On the other hand, Orbital Angular Momentum (OAM), carried by an optical vortex[10–13], is accelerating its significance recently. Since quantized OAM number ranges between minus and plus infinity, OAM would be useful for enlarging the information channels[14] in a remarked contrast with the spin angular momentum number of  $\pm 1$ .

To detect OAM of photons, a vorticity-sensitive measurement of the wave field, e.g. downstream of the specimens, is highly required. Imaging microscopy, making use of the radial Hilbert transform (RHT), is best suited for this purpose due to its sensitivity to the gradient of complex amplitude, phase and of amplitude, at the exit-face of specimens[15]. We hereafter show our experiment using the RHT which enabled us for the first time to extract the distributed OAMs and to discriminate their topological charge at the exit-face of specimens.

The RHT was invented to operate on the input complex amplitudes of two dimensional complex data in a similar manner as the Hilbert transform (HT) for one dimensional data. Three operations on the input complex amplitudes, Fourier transform, multiplication of a phase filter in the reciprocal space and inverse Fourier transform, results in complex amplitudes that equal to the convolution of the input complex amplitudes and the inverse Fourier transform of the phase filter. In the RHT, a spiral phase filter with the jump of  $2l\pi$  is used as the phase filter in the wave-number space, where  $l$  is a quantum number. This transform produces an edge enhanced image of the complex transmissivity of the specimen [Fig. 1(a)]. The RHT is sensitive to the large gradient existing in the distribution of complex amplitude.

In the RHT, the phase jump of  $2l\pi$  is preserved during the inverse Fourier transform on the spiral phase filter as shown in Fig.1 (a, b). This results in interesting sort-

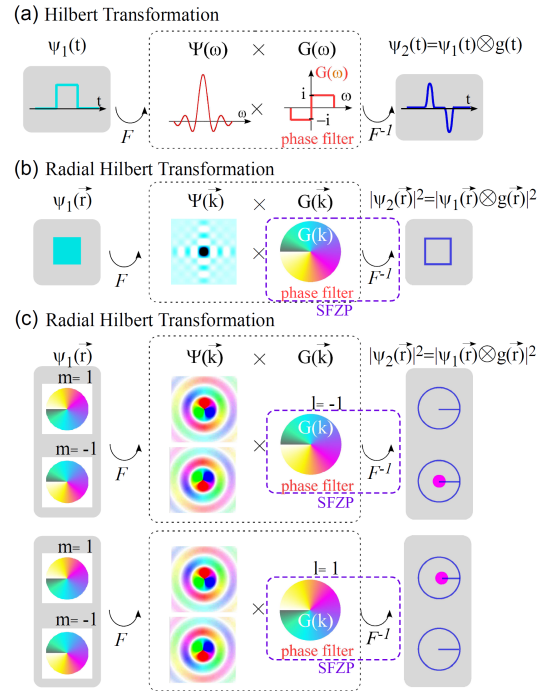


FIG. 1. (a) The filter  $G(\omega)$  in HT is a step function of  $\pi$  in angular frequency space.  $g(t)$  is inverse Fourier transform of  $G(\omega)$ . (b) The filter in RHT is a spiral phase filter with jump of  $2l\pi$  in wave-number space.  $g(\vec{r})$  is inverse Fourier transform of  $G(\vec{k})$ . Edge enhancement is observed. The function of Spiral Fresnel zone plate (SFZP) is indicated by the dotted box in purple. (c) The spiral phase anomalies with jump of  $2m\pi$  is discriminated in RHT when  $m=l$  is realized. Amplitude & phase are expressed by brightness & hue, respectively.

ing possibilities of objects having spiral phase anomalies, e.g. with the exit-face wave field of  $\psi_1(\vec{r}) \propto e^{im\phi}$  having a phase jump of  $2m\pi$  where  $m$  is a quantum number. The complex wave field at the reciprocal space is formed by the Fourier transform of the exit-face wave

field  $[\Psi(\vec{k})]$ , middle of Fig. 1(c)] which is multiplied by passing through the spiral phase filter with the complex transmissivity of  $G(\vec{k}) = e^{il\phi_k}$ , where  $\phi_k$  is the azimuthal angle in the reciprocal space. Our new theoretical analysis revealed that the output complex wave field,  $\Psi_{ml}$ , formed by the RHT shows the intensity enhancements only when the quantum numbers of  $m$  and  $l$  coincide (expressed by  $\delta_{ml}$ ) using a single image, which also has position dependences (expressed by  $\Psi_{ml}(\vec{r})$ ) in the following equation [see Fig. 1(b)],

$$\Psi_{ml}(\vec{r}) = F^{-1}[\Psi(\vec{k})e^{il\phi_k}] = \delta_{ml}\Psi_{ml}(\vec{r}). \quad (1)$$

Note that these equations are for the pure spiral phase filter and the objects with the pure spiral phase anomaly, while the neglected effect due to the distribution of attenuation will be reduced by using low-Z element for these structures. We moved on to show the possibility of determining the quantum number of a specimen using a single image while the previous theory suggested the measurability of the rotation of probability current density of the exit wave front using two images[15]. In the present experiment, a Spiral Fresnel zone plate (SFZP)[16] was utilized to function both as the lens for performing the inverse Fourier transform and as a spiral phase filter[17]. In this paper, we verify for the first time that the RHT method is powerful to sort and analyze the OAM distribution formed by the specimens.

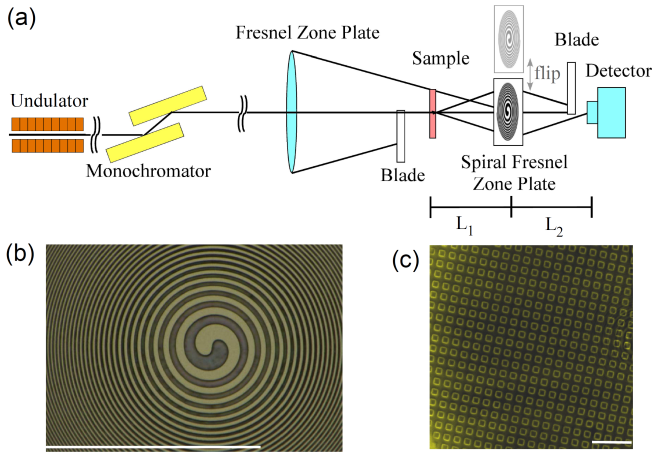


FIG. 2. (a) Setup of topological charge microscope with an objective SFZP lens placed at the focal plane of the FZP. The magnification factor of this microscope is 1.09. (b) Scanning Electron Microscope image of the SFZP used in the experiment. The scale bar corresponds to 100  $\mu\text{m}$ . (c) Edge enhanced image of copper mesh, without hosting any finite topological charge, using the topological charge microscope, with the setup shown in 2(a), exhibiting the rim of the aperture. The exposure time was 5 seconds. The scale bar corresponds to 50  $\mu\text{m}$ .

The quantum nature of OAM corresponds to (i) a complete circulation of the twisting of the vector normal to the wave front that is Poynting vector,  $\vec{S} =$

$\vec{E}^*(\vec{r}) \times \vec{H}(\vec{r}) + c.c.$  and (ii) the energy current density around an anomaly. The orientation and the number of this circulation correspond to the sign and the topological charge of the formed optical vortex.

We construct a RHT microscope using SFZP as the objective lens where the phase shift aside from the transmissivity of the specimen is observed at the image plane, which enables us to discriminate the sign and the topological charge of the generated vortices [Fig. 1(c)]. We hereafter call this microscope a topological charge microscope.

We can use two topological charge microscope images ( $l=1$  and  $l=-1$ ) obtained with reversed orientations of the SFZP objective lens. The difference of these two topological charge microscope images exhibits the distribution of rotation of Poynting vector  $\vec{S}$  at the exit-face of the specimen[15].

$$I^{l=1} - I^{l=-1} \propto i(\vec{\nabla} \times \vec{S})_z \propto i \left[ \frac{\partial \psi^*}{\partial y} \frac{\partial \psi}{\partial x} - \frac{\partial \psi^*}{\partial x} \frac{\partial \psi}{\partial y} \right] = \Omega_{xy}, \quad (2)$$

where  $\Omega_{xy}$  is a Berry curvature term. Berry curvature, the fictitious magnetic field acting on the wave[18], is an important concept applied in various fields of physics such as Hall effect, spin Hall effect[19], optical Hall effect[20], x-ray translation effect inside deformed crystals[21–24].

X-ray microscopy experiment was performed at Experimental Hutch 2 along BL29XUL[25], an undulator beamline of SPring-8 facility in Japan, using 7.71 keV x-rays from a double crystal monochromator. The higher order reflection light of monochromator was reduced by a pair of total reflection mirrors. The gap of the undulator source was set to 12.207 mm to equalize the peak intensity of 1st order harmonics to 7.71 keV. The x-ray images have been taken with an indirect x-ray image sensor[26, 27]. An objective SFZP lens was placed at the x-ray focal plane of the upstream Fresnel Zone Plate (FZP with focal length of 1.72 m) while the x-rays transmitted through the specimen between FZP and SFZP [Fig. 2(a)]. The magnification ratio of the microscope was set to be 1.09 by selecting the distances between sample-SFZP and SFZP-detector to be 1.40 m and 1.52 m, around twice the focal lengths of SFZP of 0.73 m[28]. The zone depth of 1.84  $\mu\text{m}$  was chosen for the tantalum FZP to realize  $\pi$ -phase shift at 7.71 keV. Using this setup, the wave field that corresponds to Fourier transform of the specimen's complex transmissivity is irradiated on the SFZP plane[29, 30]. This enables us to observe objects with a wide range of spatial length scales using a topological charge microscope [Fig. 1(b,c)]. Two blades were placed in front of the specimen and of the imaging detector so that the contributions from the other unnecessary orders of light from SFZP, aside from 1<sup>st</sup> order, are excluded in the setup of Fig. 2(a). The field of view was reduced to approximately one half by this order selection

of the light, approximately equalizing to the radius of SFZP which is around  $324\text{ }\mu\text{m}$ .

First, a copper mesh with the pitch of  $12.5\text{ }\mu\text{m}$ , which contains no phase anomalies or nor finite topological charge, was observed using the topological charge microscope. As shown in Fig. 1(b), only an edge enhanced image with the bright open squares at the rims of the mesh aperture was observed [Fig 2(c)].

We then move on to observe objects that yields OAMs or finite topological charges at the exit-face wave field using the topological charge and its differential microscope. For this purpose, we fabricated a specimen having four spiral phase filters at the corners of a square on a silicon substrate[31] with the maximum depth of  $19.5\text{ }\mu\text{m}$ , corresponding to the phase shift of  $2\pi$  for  $7.71\text{ keV}$  x-rays. The radii of spiral phase filters and the distances between the neighbors were set to be  $34\text{ }\mu\text{m}$  and  $80\text{ }\mu\text{m}$ , respectively. Spiral orientation of the phase filters (specimen) was defined according to the phase advance in a clock-

wise ( $m=-1$ ) or in an anti-clockwise ( $m=1$ ) orientations from downstream. This specimen was placed towards the downstream and the x-ray vortices with reversed OAM were realized among the neighbouring spiral phase filter [Fig. 3(a)].

The images of this specimen were obtained for two setting of the SFZP objective lens [Fig. 2(a)], one in an anti-clockwise ( $l=1$ ) and the other in a clockwise ( $l=-1$ ) orientation from downstream, where  $l$  corresponds to the topological charge of the SFZP [see Figs. 3(b) and 3(c)]. The result clearly indicates that the bright spots are formed at the centers of the spiral phase filters (specimen) when the quantum numbers of the spiral phase filters and SFZP coincides ( $m=l$ ) and are not when they are different ( $m=-l$ ). The results shown in Figs. 3(b) and 3(c) agree well with eq. (1). The attenuation through these structures was not taken into account in eq.(1), but this effect was not significant as shown in these figures. The differential image obtained from these two images, which visualizes the distribution of Berry curvature at the exit-face of the specimen, is shown in Fig. 3(d). Remarkable structures at the centers and at the rims of the spiral phase filters were exhibited which were also clearly visible in the calculated differential image shown in Fig. 3(e), derived from eq. (2). Note that Fig. 3(e) was calculated by taking account of the attenuation through the structures of spiral phase filters in the specimen.

The developed microscope, which visualizes the spatial distributions of OAM from one or two images, is free from the extremely precise alignment. The present microscope will open the door of various OAM related researches e.g., x-ray OAM-induced dichroism[2] or further modification of the selection rules that govern the transfer of OAM between valence electrons and photons[1] and so on. The chirality research[32] in atomic resolution would be also accelerated.

### Acknowledgments

Experiments at SPring-8 BL29XU have been performed with the approval of RIKEN (under proposal numbers of 20170065). Y. K. express a sincere gratitude to Drs. L. Szyrwił and A. Takeuchi for discussions.

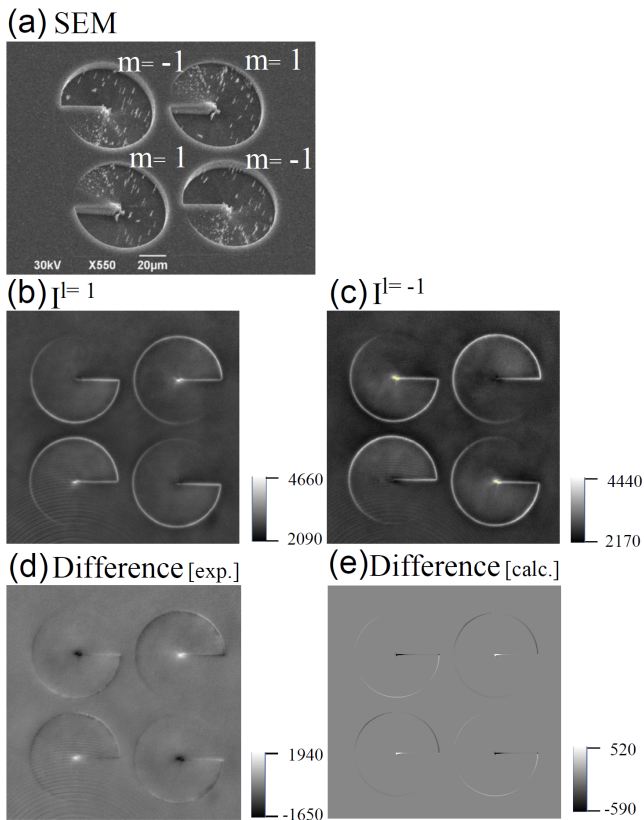


FIG. 3. (a) Image of multiple spiral phase filters on the corners of a square by Scanning Electron Microscope (SEM) with the magnification factor of  $M=550$ . Topological charge microscope images obtained with the SFZP objective lens having the quantum OAM number of (b)  $l=1$  (anti-clockwise) and (c)  $l=-1$  (clockwise from downstream) and the exposure time of 5 seconds. (d) Differential microscope image ( $I^{l=1} - I^{l=-1}$ ) of two images in 3(b) and 3(c). (e) Calculated differential microscope image using eq. (2).

- 
- [1] C. T. Schmiegelow, *et al.* Nature Communications **7**, 129981-129986 (2016).
  - [2] M. V. Veenendaal, and I. McNulty, Phys. Rev. Lett., **98**, 157401 (2007).
  - [3] S. W. Hell, and J. Wichmann, Opt. Lett. **19**, 780 (1994).
  - [4] S. Hell, Nature BioTechnology **21**, 1347 (2003).
  - [5] Y. Kohmura, *et al.* Appl. Physics Lett. **112**, 1231031 (2018).

- [6] A. Ambrosio, *et al.* Nat. Com., **3**, 989 (2012).
- [7] F. Takahashi, *et al.* Scientific Reports, **6**, 21738 (2016).
- [8] K. Toyoda, *et al.* Nano Letters, **12**, 3645 (2012).
- [9] K. Toyoda, *et al.* Phys. Rev. Lett., **110**(14), (2013).
- [10] M. Padgett, J. Courtial and L. Allen, Physics Today, **57** (5), 35 (2004).
- [11] M. Zürch, *et al.* Nature Physics **8**, 743 (2012).
- [12] A. G. Peele, *et al.* Opt. Lett. **27**, 1752 (2002).
- [13] Y. Taira, *et al.* Scientific Reports **7**, 5018 (2017).
- [14] Z-Y. Zhou, *et al.* Light: Science & Applications **5**, e16019 (2016).
- [15] R. Juchtmans, *et al.*, Phys. Rev. A, **94**, 023838 (2016).
- [16] A. Sakdinawat, *et al.* Opt. Lett. **32**, 2635-2637 (2007).
- [17] SFZP is a modified FZP, designed to function both as the lens and as the spiral phase filter, having the complex transmissivity expressed in the following equation
- $$\text{SFZP}_l(r, \phi) = \exp(il\phi - \frac{i\pi r^2}{\lambda f}), \quad (3)$$
- where  $l$ ,  $\phi$ ,  $\lambda$  and  $f$  are the OAM quantum number, the azimuthal angle around the center of vortex, the x-ray wavelength and the focal length of SFZP[16], respectively. The fabricated SFZP is binalized from the function expressed above.
- [18] H. Kurosawa, K. Sawada, and S. Ohno, Phys. Rev. Lett., **117**, 083901 (2016).
- [19] O. Hosten, & P. Kwiat, Science. **319**, 787 (2008).
- [20] M. Onoda, S. Murakami, & N. Nagaosa, Phys. Rev. Lett. **93**, 083901 (2004).
- [21] K. Sawada, S. Murakami, & N. Nagaosa, Phys. Rev. Lett. **96**, 154802 (2006).
- [22] Y. Kohmura, K. Sawada, & T. Ishikawa, Phys. Rev. Lett. **104**, 244801 (2010).
- [23] Y. Kohmura, K. Sawada, S. Fukatsu, & T. Ishikawa, Phys. Rev. Lett. **110**, 057402-1 (2013).
- [24] D. Takei, Y. Kohmura, K. Sawada, & T. Ishikawa, Optics Express **24**(21), 24544 (2016).
- [25] K. Tamasaku, *et al.* Nucl. Instrum. Methods Phys. Res. **A467-468**, 686-689 (2001).
- [26] T. Kameshima, *et al.*, AIP Conf. Proc., **1741**, 040033 (2016).
- [27] The x-ray images have been taken with an indirect x-ray image sensor composed of a fluorescence screen made from a LuAG single crystal, an optical lens system and a CMOS camera[26]. The effective pixel size of the detector was 325 nm.
- [28] The utilized FZP and SFZP were fabricated by the Shinko-Seiki Corp. (Kobe, Japan). The specifications of FZP and SFZP were the diameter of  $2r_N = 664 \mu\text{m}$  &  $648 \mu\text{m}$ , the first zone radius of  $r_1 = 16.6 \mu\text{m}$  &  $10.8 \mu\text{m}$ , the outermost zone width of  $\Delta r_N = 0.415 \mu\text{m}$  &  $0.18 \mu\text{m}$ , number of zones of 400 & 900, respectively. The 7.71keV x-ray focal lengths are 1.72 m and 0.73 m, respectively. These ZPs were formed on a membrane on the 500  $\mu\text{m}$  silicon substrate, back edged to have the thickness of  $\simeq 80 \mu\text{m}$ .
- [29] J. W. Goodman, *Introduction to Fourier Optics*, 2nd Edition, McGraw-Hill (1996).
- [30] A topological charge microscope requires the Fourier transform of the specimen's complex transmissivity to be irradiated on the SFZP [Fig. 1(b, c)]. The propagated wave field between the specimen and the SFZP, however, is affected by the additional Fresnel diffraction term downstream of the specimen. This term is cancelled by placing a focusing optics upstream of the specimen and by placing the SFZP objective lens at the corresponding focal plane[16, 29] as shown in Fig. 2(a).
- [31] The specimen with four spiral phase filters were fabricated by the Shinko-Seiki Corp. (Kobe, Japan) on a membrane formed on a silicon substrate back edged to have the thickness of  $\simeq 80 \mu\text{m}$ .
- [32] W. Brullot, *et al.* Sci. Adv. **2**, e15013491 (2016).